Using CFD to derive reduced order models for heat transfer in particle curtains

Sepideh Afshar* and Madoc Sheehan

Department of Chemical Engineering,
James Cook University,
Townsville, Queensland 4811, Australia
Email: sepideh.afshar@my.jcu.edu.au
Email: Madoc.Sheehan@jcu.edu.au
*Corresponding author

Amir Fazlollahi

Laboratoire Le2I,
Université de Bourgogne,
Le Creusot, France
Email: Fazlollahi@gmail.com

Abstract: 3-D Eulerian-Eulerian CFD is used to simulate convective heat transfer in free falling particle curtains. Total heat loss for curtaining particles is compared to heat loss for isolated single particles. Spherical silica particles with density of 2,634 kg/m^3 at 400 K (200 μm, 400 μm and 600 μm) flow at approximately 0.041 kg/s to 0.2 kg/s through a narrow slot in a rectangular box (0.45 m × 0.9 m × 0.225 m) filled with ambient air. The slot sizes through which the particles enter the rectangular box were 10 to 80 mm wide. Modifying the slot size at 0.041 kg/s for 400 μm particles can lead to 13% increases in rates of convective heat transfer per unit mass. A reduced order model was developed to predict the centreline temperatures of particles in the falling curtains. The drag coefficient in the ROM was varied to suit a range of particle sizes and mass flow rates.

Keywords: particle; computational fluid dynamics; heat transfer; convection; Eularian-Eularian; reduced order model; curtain; residence time; drag; drying.

Reference to this paper should be made as follows: Afshar, S., Sheehan, M. and Fazlollahi, A. (2015) 'Using CFD to derive reduced order models for heat transfer in particle curtains', *Progress in Computational Fluid Dynamics*, Vol. 15, No. 2, pp.71–80.

Biographical notes: Sepideh Afshar received her Master in Chemical Engineering in Science and Research Branch University of Tehran in Iran. She is currently a PhD researcher at James Cook University. Her interest is computational fluid dynamics (CFD) in drying industry. Her thesis is focused on CFD simulations of particle curtains and their integration into multi-scale dryer models.

Madoc Sheehan received his PhD degree from the University of Manchester Institute of Science and Technology (UMIST) in 1999. He is currently a Chemical Engineering Senior Lecturer at James Cook University. He has won national awards for teaching excellence and has published educational research on curriculum development and education for sustainability. He has had extensive experience in mathematical modelling and drying, and has published more than 40 papers in these fields. He has extensive experience in industry-scale model validation, and the development of multi-scale modelling approaches for solid/gas systems.

Amir Fazlollahi received his BS in Computer Software Engineering from Shiraz University, Iran in 2009 and MS in Computer Vision from University of Burgundy, France in 2011. He is currently pursuing his PhD in Medical Image Processing at University of Burgundy, France. His research interest includes medical and biomedical image analysis, pattern recognition, and computer vision.

This paper is a revised and expanded version of a paper entitled 'Using CFD to simulate heat transfer in particle curtains' presented at 9th International Conference on CFD in the Minerals and Process Industries, Melbourne, 10–12 December 2012.

Copyright © 2015 Inderscience Enterprises Ltd.

1 Introduction

A particle curtain is defined as a continuous stream of particles, falling under the influence of gravity, off the edge of a surface or through a slot of fixed dimensions. This type of phenomena occurs in many different industrial and environmental situations, including a variety of solids cascading off rotating flights in rotary dryers, molten salts in solar thermal receivers, solids flowing off conveyors, chutes and buckets, as well as droplets in waterfalls. They are particularly important in industrial drying operations where optimising heat and mass transfer between the cascading particles and the drying medium is essential for reducing operating costs. Furthermore, prediction of particle curtain drag forces is important to estimating unit residence times. Numerous empirical models have been developed to predict curtain solid transport (predominantly drag) (Schiller and Naumann, 1933; Wen and Yu, 1966; Baker, 1992) and drying (i.e., heat and mass transfer) (Ranz, 1952). In particular, the use of single particle models is dominant.

Ogata et al. (2001) compared the behaviour of free falling curtains and single particles in a particle jet in terms of vertical velocity. It was found that the velocity of particles within curtains was higher than the velocity of comparable single particles. Ogata et al. (2001) and Hurby et al. (1988) suggested that this was due to the surrounding air being entrained within the curtain, reducing drag.

Hurby et al. (1988) studied heat transfer in freely falling curtains (0.02, 0.04 kg/s) of spherical Norton Master Beads^{TM} and compared experimental observations to 2-D Eulerian-Lagrangian simulations. The results showed that heat losses were lower at high flow rate (0.04 kg/s) when compared to low mass flow rate (0.02 kg/s).

Wardjiman et al. (2008, 2009) studied the shape of particle curtains in terms of divergence and convergence downstream of the discharge. It has been observed that varying initial curtain widths at the discharge point can lead to both diverging and converging curtain behaviour. It was found that for small initial curtain widths (i.e., 2 cm) the shape of the falling curtain diverged whereas at larger curtain widths (i.e., 8 cm) the curtain converged. The convexity behaviour has been attributed to variation in air pressure. 3-D Eulerian-Eulerian CFD reported in these papers was found to reasonably match experimental results for curtain shape under both stagnant and cross flow air conditions.

Wardjiman et al. (2009) studied heat transfer in a particle curtain experimentally and numerically. Experiments were conducted in a rectangular tunnel in which particles were heated with hot air. Temperatures of both particles within curtain, and the gas were collected. Wardjiman et al. (2009) used an individual sample cup to obtain temperatures versus curtain height. However, the bulk temperature profile across the entire curtain was not obtained. These experimental results were compared to numerical simulations based on the single particle model. It is worth noting that the single particle model has been commonly used in approximating curtain behaviour. Unfortunately the single particle thermal model in Wardjiman et al.'s (2009) work was not well matched with measured air temperatures from the experiments although it was stated that the match between particle temperatures was better.

To the authors best knowledge, all examples of geometric modelling of flighted rotary dryers have utilised the single particle model to represent curtain behaviour (see for example, Britton et al., 2006). This model has been essential to estimating airborne flights times and calculating mean residence times. Baker (1992) demonstrated that the single particle model overestimated the drag experienced by the particles within the curtains. To improve predictions of particle movement using the single particle model, Baker modified the magnitude of the drag coefficient and assumed the curtains behaved as flat plates. This led to improved results, but its calculation was complicated by a lack of data characterising the curtain properties (voidage and thickness). Baker's work demonstrates that the single particle model is a good candidate for developing a reduced order model to represent curtain behaviour. Reduced order models (ROM) have been used in modelling particulate systems such as fluidised beds (Thanh et al., 2008).

In this paper the Eulerian-Eulerian approach has been used to model heat loss in falling particle curtains. The effects of particle mass flow, particle size and particle slot opening size were investigated using analysis of variance (ANOVA) techniques. Centreline particle temperature profiles from CFD simulations were also compared to those derived using the single particle model. A single particle reduced order model was derived to better represent heat transfer in particle curtains. Conditions leading to maximum heat transfer in particle curtains are examined.

2 CFD model

A 3-D Eulerian-Eulerian model was used to simulate gas-particle interactions in falling particle curtains. The simulations were performed using ANSYS CFX V13.0 CFD software.

The model equations in Eulerian-Eulerian approach are based on the continuity, momentum, energy conservation principles at steady state:

2.1 Continuity equations

Gas phase:

$$\frac{\partial(\alpha_g \rho_g)}{\partial t} + \nabla.(\alpha_g \rho_g \vec{v}_g) = 0, \tag{1}$$

Solid phase:

$$\frac{\partial(\alpha_s \rho_s)}{\partial t} + \nabla.(\alpha_s \rho_s \vec{v}_s) = 0. \tag{2}$$

2.2 Momentum equations

Gas phase

$$\begin{aligned} &\frac{\partial}{\partial t}(\alpha_g \rho_g \vec{v}_g) + \nabla.(\alpha_g \rho_g \vec{v}_g \vec{v}_g) \\ &= \nabla.\bar{\bar{\tau}}_g - \alpha_g \nabla \mathrm{P} - \alpha_g \rho_g \vec{g} + \beta(\vec{v}_s - \vec{v}_g), \end{aligned} \tag{3}$$

Solid phase

$$\begin{aligned} &\frac{\partial}{\partial t}(\alpha_s \rho_s \vec{v}_s) + \nabla.(\alpha_s \rho_s \vec{v}_s \vec{v}_s) \\ &= \nabla.\bar{\bar{\tau}}_s - \alpha_s \nabla \mathrm{P} - \nabla \mathrm{P}_s - \alpha_s \rho_s \vec{g} + \beta(\vec{v}_g - \vec{v}_s). \end{aligned} \tag{4}$$

Stress tensors:

$$\bar{\bar{\tau}}_g = \alpha_g \mu_g \left(\nabla \vec{v}_g + \nabla \vec{v}_g^T\right) + \alpha_g \left(\lambda_g + \frac{2}{3}\mu_g\right) \nabla.\vec{v}_g \bar{\bar{\mathrm{I}}}, \tag{5}$$

$$\bar{\bar{\tau}}_s = \alpha_s \mu_s \left(\nabla \vec{v}_s + \nabla \vec{v}_s^T\right) + \alpha_s \left(\lambda_s + \frac{2}{3}\mu_s\right) \nabla.\vec{v}_s \bar{\bar{\mathrm{I}}}, \tag{6}$$

Bulk viscosity:

$$\lambda_s = \frac{4}{3}\alpha_s^2 \rho_s d_s g_0 (1 + e_s) \sqrt{\frac{\Theta_s}{\pi}} \tag{7}$$

Solid pressure:

$$P_s = \alpha_s \rho_s \Theta_s \left(1 + 2 g_0 \alpha_s (1 + e_s)\right) \tag{8}$$

Shear viscosity:

$$\begin{aligned} \mu_s = &\frac{4}{5}\alpha_s \rho_s d_s g_0 (1 + e_s) \sqrt{\left(\frac{\Theta_s}{\pi}\right)} \\ &+ \frac{5\sqrt{\pi}}{48}\left(\frac{\rho_s d_s}{(1 + e_s)\alpha_s g_0}\right)\left[1 + \frac{4}{5}(1 + e_s) g_0 \alpha_s\right]^2 \sqrt{\Theta_s} \end{aligned} \tag{9}$$

Radial distribution function (Gidaspow, 1994):

$$g_0 = \left[\frac{3}{5}\left[1 - \left(\frac{\alpha_s}{\alpha_{s,\max}}\right)^{\frac{1}{3}}\right]\right]^{-1}, \tag{10}$$

$\alpha_{s,\max} = 0.65$

Granular temperature:

$$\Theta_s = \frac{1}{3}\overline{v_s' v_s'} \tag{11}$$

2.3 Energy equation

$$\begin{aligned} &\frac{\partial}{\partial t}(\alpha_q \rho_q h_q) + \nabla.(\alpha_q \rho_q \vec{v}_q h_q) \\ &= \alpha_q \frac{\partial P_q}{\partial t} - \nabla.\vec{q}_q + Q_{pq} \end{aligned} \tag{12}$$

In which h_q is specific enthalpy of q^{th} phase, $\nabla.\vec{q}_q$ is the heat flux and Q_{pq} is the intensity of heat exchange between the p^{th} and q^{th} phases.

2.4 Heat transfer equations

Equations of convective heat transfer between particle curtains and air can be written as follows:

$$Q_{sg} = hA(T_s - T_g) \tag{13}$$

where h is convective heat transfer coefficient, A is the area of particles in curtain.

$$h = \frac{Nu.k_g}{d_s} \tag{14}$$

The Ranz-Marshall correlation (Ranz, 1952) was used to describe heat transfer coefficient characterising correlation between air and particles:

$$Nu = 2 + 0.6 Re^{0.5} Pr^{0.3} \tag{15}$$

$$Pr = \frac{C_{pg}\mu_g}{k_g} \tag{16}$$

$$Re = \frac{\alpha_s \rho_s d_s \left|\vec{v}_s - \vec{v}_s\right|}{\mu_g} \tag{17}$$

2.5 Drag model

Interphase drag (β) is an important characteristic and has been the subject of numerous investigations (Pei et al., 2012).The classic approach to modelling these dilute two-phase systems is the Gidaspow model which is a combination of two older model developed by Wen-Yu and Ergun (Gidaspow, 1994).

$$\beta = \left(1-\varphi_{gs}\right)\beta_{Ergun} + \varphi_{gs}\beta_{Wen\text{-}Yu} \tag{18}$$

$$\varphi_{gs} = \frac{\arctan\left[150\times 1.75\left(0.2-\alpha_s\right)\right]}{\pi} + 0.5 \tag{19}$$

$$\beta_{Ergun} = 150\frac{\alpha_s^2\mu_g}{\alpha_g d_s^2} + 1.75\frac{\alpha_s\rho_g\left|\vec{v}_g-\vec{v}_s\right|}{d_s} \qquad \alpha_g < 0.8 \tag{20}$$

$$\beta_{Wen\text{-}Yu} = \frac{3}{4}C_D\frac{\alpha_s\rho_g}{d_s}\left|\vec{v}_g-\vec{v}_s\right|\alpha_g^{-2.65} \qquad \alpha_g \geq 0.8 \tag{21}$$

The particle drag model (C_D) was evaluated using the commonly used Schiller-Naumann (1933) equation:

$$C_D = \begin{cases} \dfrac{24}{\alpha_g Re}\left[1+0.15\left(\alpha_g Re\right)^{0.687}\right] & Re < 1{,}000 \\ 0.44 & Re \geq 1{,}000 \end{cases} \tag{22}$$

where

$$Re = \frac{\rho_g d_s\left|\vec{v}_g-\vec{v}_s\right|}{\mu_g} \tag{23}$$

2.6 Turbulence model

The k-ε turbulence model has been frequently used for multi-phase simulation and has been shown to provide close agreement between experiments and simulations (Papadikis et al., 2009; Wardjiman et al., 2008, 2009).

Continuous phase turbulence model (k-ε model)

$$\mu_{tr,g} = 0.09\frac{\rho k_g^2}{\varepsilon_g} \tag{24}$$

Turbulent kinetic energy

$$\frac{\partial}{\partial t}\left(\alpha_g\rho_g k_g\right) + \nabla.\left(\alpha_g\left(\rho_g\vec{v}_g k_g - \left(\mu_g + \frac{\mu_{tr,g}}{\sigma_k}\right)\nabla k_g\right)\right) = \alpha_g\left(G_{k,g} - \rho_g\varepsilon_g\right) \tag{25}$$

Turbulent dissipation rate

$$\frac{\partial}{\partial t}\left(\alpha_g\rho_g\varepsilon_g\right) + \nabla.\left(\alpha_g\left(\rho_g\vec{v}_g\varepsilon_g - \left(\mu_g + \frac{\mu_{tr,g}}{\sigma_k}\right)\nabla\varepsilon_g\right)\right) = \alpha_g\frac{\varepsilon_g}{k_g}\left(C_{\varepsilon 1}G_{k,g} - C_{\varepsilon 2}\rho_g\varepsilon_g\right) \tag{26}$$

where $C_{\varepsilon 1} = 1.44$, $C_{\varepsilon 1} = 1.92$, $\sigma_k = 1.0$ and $\sigma_\varepsilon = 1.3$.

Generation of turbulent kinetic energy

$$G_{k,g} = \mu_{tr,g}\nabla\vec{v}_g.\left(\nabla\vec{v}_g + \nabla\vec{v}_g^T\right) - \frac{2}{3}\nabla.\vec{v}_g + \left(3\mu_{tr,g}\nabla.\vec{v}_g + \rho_g k_g\right) + G_{kb,g} \tag{27}$$

Turbulent buoyancy

$$G_{kb,g} = \frac{\mu_{tr,g}}{\rho_g}g.\nabla\rho_g \tag{28}$$

Dispersed phase turbulence model (zero-equation model)

$$\mu_{tr,s} = \frac{\rho_s}{\rho_g}\mu_{tr,g} \tag{29}$$

3 Single particle model

Drag and gravitational forces are the most important forces acting on a single particle. The general equation of motion for a single particle can then be writhen as:

$$F_{net} = F_G - F_D \tag{30}$$

$$m_s\frac{dv_s}{dt} = F_G - F_D \tag{31}$$

In which:

$$F_G = m_s g \tag{32}$$

$$F_D = C_D A_{xs}\frac{1}{2}\rho_g v_s^2 \tag{33}$$

Thus:

$$m_s\frac{dv_s}{dt} = m_s g - C_D A_{xs}\frac{1}{2}\rho_g v_s^2 \tag{34}$$

The initial velocity of the single particle was assigned the same initial velocity as the curtaining particles at the inlet. Heat transfer in the single particle model was described by equations (13) to (17).The temperature of a single particle was calculated by numerical integration of equation (35):

$$\frac{dT_s}{dt} = \frac{A_s\times h}{m_s\times C_p}\left(T_g - T_s\right) \tag{35}$$

In the single particle model it was assumed that the gas temperature remains constant at 300 K. The drag coefficient (C_D) used in single particle model was calculated using the same relations as the Eulerian-Eulerian simulation [equation (22)].

4 Computational set-up

The geometry consists of a rectangular box with varying slot width in X direction from 10 to 80 mm and constant slot length in the Z direction of 150 mm (Figure 1).

Figure 1 Schematic diagram of simulation domain (see online version for colours)

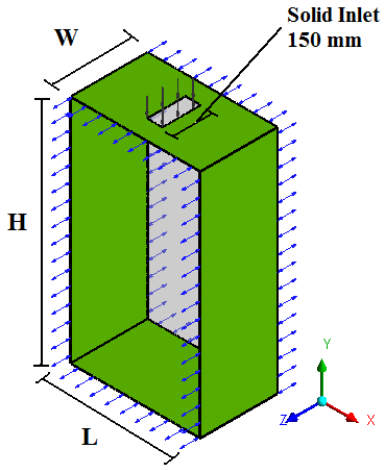

Notes: L = 450 mm, H = 900 mm and W = 225 mm

The model was solved with 4 mm multizone mesh size. The details of mesh dependency will be described further in this paper.

The simulation initial conditions are given in Table 1.

Table 1 Initial conditions of simulation domain

Solid volume fraction at solid inlet	0.52
Solid inlet temperature	400 K
Initial gas temperature	300 K
Air velocity at solid inlet	0 m/s
Solid mass flow rate at solid inlet	0.041, 0.1, 0.2 kg/s

5 Average heat loss in particle curtain

The heat loss is characterised as the total heat loss of the falling particles from the entrance to the landing zone (in this case located 0.8 m down from the entrance).

Equation (36) was used to determine the total heat loss per unit mass within the curtain.

$$\hat{Q} = C_p \overline{\Delta T} \tag{36}$$

where $\hat{Q}$ is the total heat loss per unit mass, C_p is the heat capacity of sand (Incropera and DiWitt, 2002) and $\overline{\Delta T}$ is the average temperature difference within the falling height $(\overline{T}_2 - T_{inlet})$. In which $\overline{T}_2$ is the average temperature of the particle curtain in a ZX plane 0.8 m down from the entrance. The inlet temperature (T_{inlet}) is well-defined. The outlet temperature is more challenging to determine.

Typically integration is used for the calculation of average properties. The temperature of the particle curtain at the defined plane is described by numerical integration of the data [equation (37)], using mass flow rate as a weight function:

$$\overline{T}_2 = \frac{\int_{x=0}^{x=W}\int_{z=0}^{z=L} m^o T_{xz}\, dzdx}{\int_{x=0}^{x=W}\int_{z=0}^{z=L} m^o\, dzdx} \tag{37}$$

Integration can be defined as an infinite sum. Therefore the integration form can be replaced by summation of values [equation (38)]

$$\overline{T}_2 = \frac{\sum_{z=0}^{z=L}\sum_{x=0}^{x=W} m^o_{xz} T_{xz}}{\sum_{z=0}^{z=L}\sum_{x=0}^{x=W} m^o_{xz}} \tag{38}$$

In equations (37) and (38) m^o_{xz} and T_{xz} are mass flow rate and temperature of sand at each node of simulation in the defined ZX plane.

In each node of the ZX plane particularly the outside edges, negative and positive values of mass flow rate occur (Figure 2). Only mass flow values for the downward particles were considered.

Figure 2 Sand mass flow rate vectors at ZX plane, 0.8 m down from the entrance (see online version for colours)

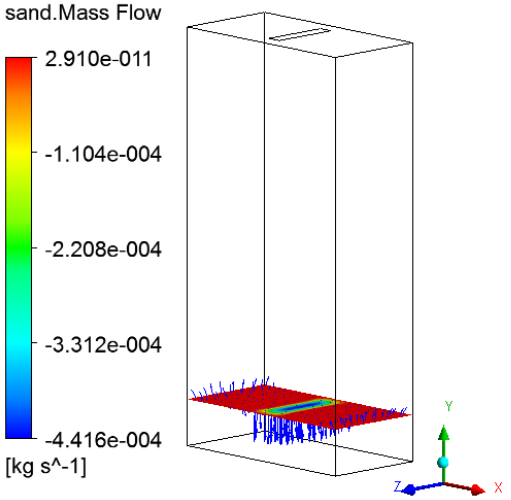

6 Mesh dependency

The accuracy of results depends on the quality of mesh size used in simulations. Kim et al. (2009) investigated mesh dependency in their modelling of a pilot scale solid particle receiver. It was found that mesh size in the CFD simulation has an important effect on determining the thickness of the curtain.

In this paper mesh dependency was carried out on the described geometry at different mesh sizes (3 mm, 4 mm, 5 mm, 6 mm, 7 mm and 8 mm) with a mass flow rate of 0.041 kg/s. Different slot sizes (10 mm, 60 mm and 80 mm) were investigated (Figure 3). Average heat loss per unit mass as, described in equation (34), was used as the convergence criteria. A mesh size of 4 mm with 1,449,225 elements was utilised in all simulations.

Figure 3 Heat loss predictions using the indicated element sizes (see online version for colours)

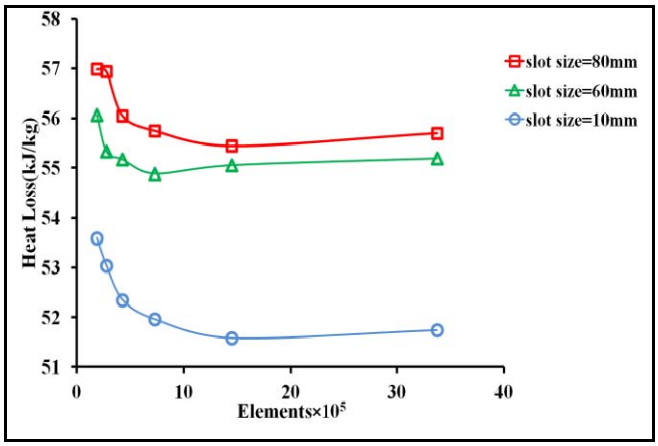

7 Results

7.1 Effects on average heat loss

Figure 4 shows a selection of results comparing CFD calculated heat losses per unit mass at different slot sizes (10 mm, 30 mm, 60 mm and 80 mm), mass flow rates (0.041 kg/s, 0.1 kg/s and 0.2 kg/s) and particle sizes (200 µm, 400 µm and 600 µm). Similar trends in the effect of particle size (0.041 kg/s) were observed at higher mass flow rates of 0.1 kg/s and 0.2 kg/s.

Figure 4 Heat loss comparison at slot sizes of 10 mm, 30 mm, 60 mm, 80 mm, particle sizes of 200 µm, 400 µm and 600 µm and mass flow rates of 0.041 kg/s,0.1 kg/s and 0.2 kg/s (see online version for colours)

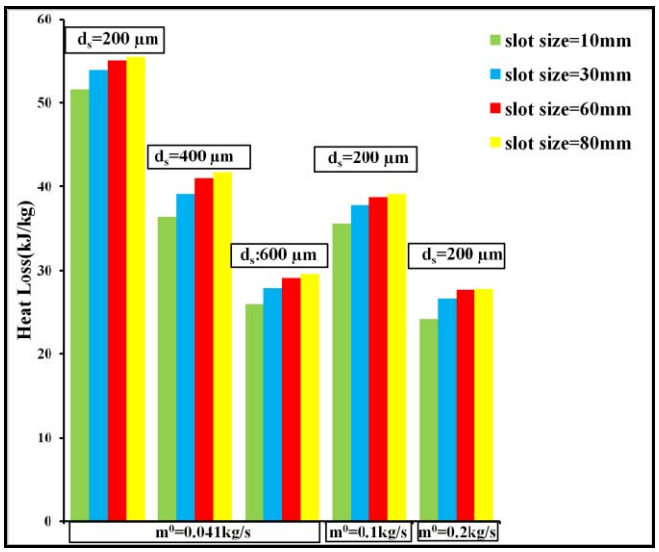

A three way ANOVA was used to evaluate the effect of variables particle size (at three levels of 200 µm, 400 µm and 600 µm), mass flow rate (at three levels of 0.041 kg/s, 0.1 kg/s, 0.2 kg/s) and slot opening size (at four levels of 10 mm, 30 mm, 60 mm and 80 mm) on heat loss. ANOVA results were generated with SPSS 19.0 (Table 2).

The results showed that all three variables of slot opening size, particle size and mass flow rate have significant effect on heat loss, as P values (Sig.) are less than 0.05, but the top three most significant effects were mass flow rate, particle size and the interaction of mass flow rate and particle size. As an example Figure 5 shows the interaction effect between mass flow rate and particle size. It also shows the highest effect is at lowest mass flow rate and smallest particle size (200 µm).

Table 2 Summary of results obtained by ANOVA

Source	*Sum of squares*	*Mean square*	*F*	*Sig.*
SlotSize	8.964×10^7	2.988×10^7	1,405.447	0
d_s	1.831×10^9	9.157×10^8	4.307×10^4	0
m^o	2.199×10^9	1.099×10^9	5.170×10^4	0
$d_s \times m^o$	2.546×10^8	6.364×10^7	2.993×10^3	0
SlotSize × m^o	1.833×10^5	3.056×10^4	1.437	0.279
SlotSize × d_s	2.271×10^6	3.785×10^5	1.780×10	0
Error	2.551×10^5	2.126×10^4		
Total	3.783×10^{10}			

Figure 5 Average heat loss for interaction effect of particle size and mass flow rates (see online version for colours)

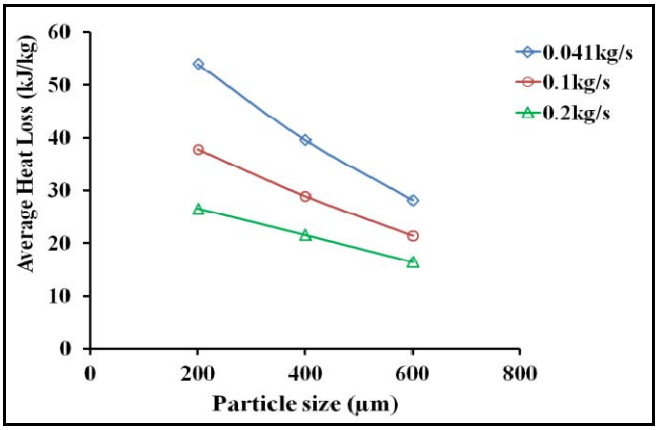

Figure 6 shows a comparison of heat loss per unit mass versus slot widths at the different mass flow rates for particle size of 200 µm. It was observed that there is a critical condition upon which further increases in slot width do not lead to increases in heat loss per unit mass. It can be seen that heat loss is higher at lower mass flow rate (0.041 kg/s), however heat loss is almost independent of slot size at larger slot sizes of 60 mm and 80 mm in the same mass flow rate.

Figure 6 Heat loss per unit mass for different slot sizes at mass flow rates of 0.041 kg/s, 0.1 kg/s and 0.2 kg/s for particle size of 200 µm (see online version for colours)

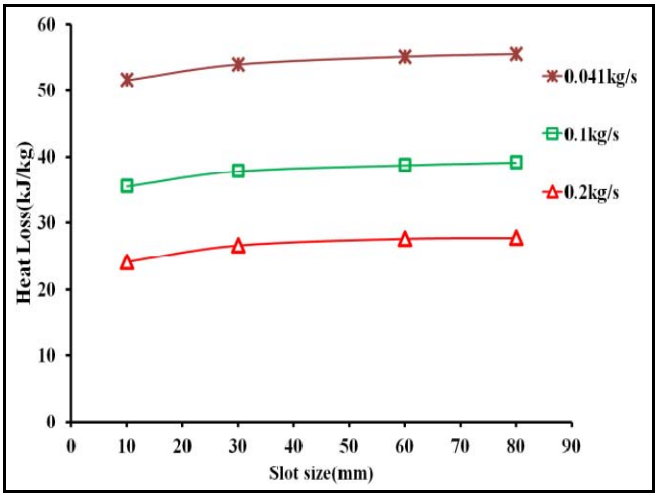

7.2 Centreline temperature profiles

The change in particle temperature over falling distance is an important characteristic in curtain thermal behaviour. Both the single particle model and CFD simulations can be used to generate such profiles, although it is well known that the single particle models have deficiencies. In this work we make the reasonable assumption that the CFD simulation results are a better approximation to the real system. In preliminary work, the temperature profiles of falling particles calculated using our CFD approach have been compared to experimental results (Afshar and Sheehan, 2013). It was demonstrated that CFD provides a good comparison to experimental results for small particle sizes such as around 290 µm. At larger particle sizes the differences between the CFD model and experimental data were increased. This might be caused by the use of turbulence zero-equation model for dispersed phase, or alternatively drag model deficiencies might exist. However for all particle sizes the CFD results were an improvement over the single particle model.

Figures 7 to 9 shows a selection of temperature profile comparisons between single particle simulations and CFD values for the centreline temperature of particles in the curtains. The temperature of single particle and particles in curtain has been non-dimensionalized:

$$T^* = \frac{T - T_{f-CFD}}{T_0 - T_{f-CFD}},$$

in which $T_{f\text{-}CFD}$ is the final temperature of particles in curtain after 0.8 m falling distance and T_0 is 400 K.

Figure 7 Temperature comparison between single particle and particles in curtain in 10 mm slot at three 0.041, 0.1 and 0.2 kg/s mass flow rates and particle size of 200 µm (see online version for colours)

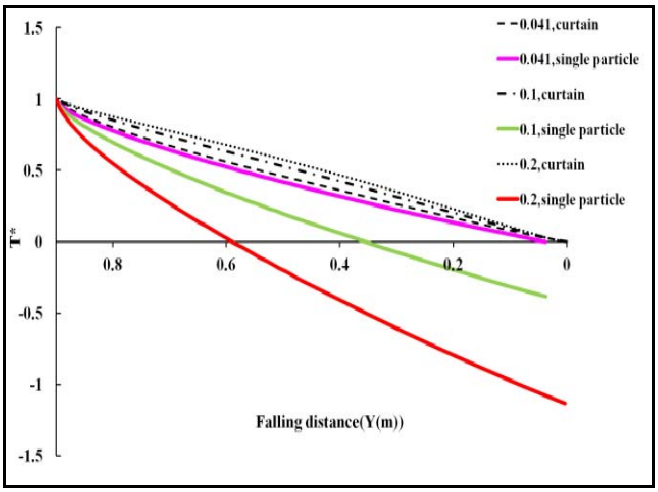

Figure 8 Temperature comparison between single particle and particles in curtain in 60 mm slot at three 0.041, 0.1 and 0.2 kg/s mass flow rates and particle size of 200 µm (see online version for colours)

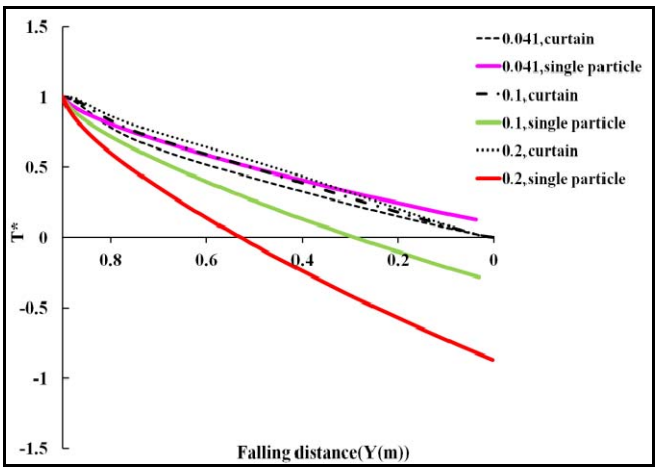

Figure 9 Temperature comparison between single particle and particles in curtain in 80 mm slot at three 0.041, 0.1 and 0.2 kg/s mass flow rates and particle size of 200 μm (see online version for colours)

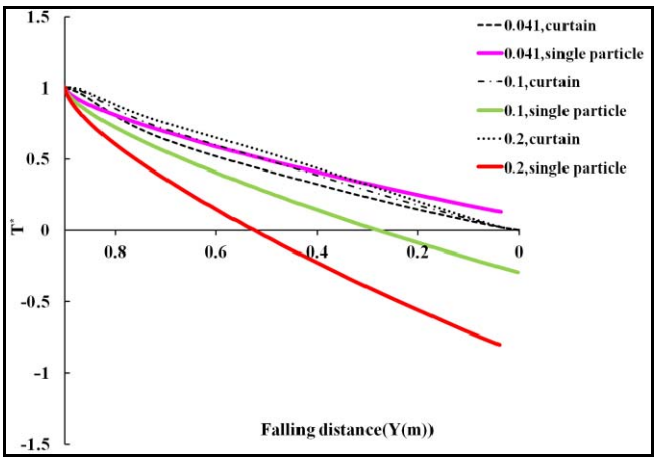

It was found that the heat loss per unit mass of particles in curtain is less than the single particle particularly at higher mass flow rates (0.1 kg/s and 0.2 kg/s) and there are smaller temperature differences between single particle simulations and CFD results for particles in the curtain at low mass flow rate (0.041 kg/s).

It can be seen that for narrow slots (10 mm), in all cases the single particle loses heat faster than its equivalent curtain. As the slot width widens or mass flow rate decreases this effect is less pronounced. In fact, in the low mass flow rate (0.041 kg/s) and wide slot (60 mm and 80 mm) simulations this effect is reserved and the single particle loses heat at a slower rate. Under these low flow, wide slot conditions the curtain shape is convergent (narrows as it falls) rather than divergent, which seems to be a significant factor.

As illustrated in Figures 7 to 9, the modelled temperature behaviour of a single particle is different to that of particles in the curtain. The aim of this section is to describe the development of the single particle model as a ROM for predicting the temperature of falling particle curtains. The CFD models are used as the basis from which the ROM is derived. The first step in developing a ROM is to identify the controlling factors and identify the variables of the single particle model that could be modified in order to reproduce the thermal behaviour of particles in curtains.

The top two most significant effects were identified as mass flow rate and particle size. These two effects were considered enough for developing the ROM and lesser effects were ignored. In terms of the single particle model parameters, Baker (1992) suggests that the magnitude of the particle drag would be the most appropriate parameter to vary. Furthermore, Hruby et al. (1988) also suggested that for hot particles the magnitude of drag is different to that of cold particles. From a practical perspective, because air is entrained within the curtain as it falls there is a difference between the drag experienced by a single particle and that in a particle curtain.

In the ROM, the magnitude of the drag coefficient is altered by introducing the parameter B into the drag coefficient correlation [equation (22)]:

$$C_D\big|_{ROM} = B \times \frac{24}{Re}\left[1 + 0.15(Re)^{0.687}\right] \tag{39}$$

In order to obtain initial estimates of the value of B, a trial and error study was carried out using the observed temperature profiles for different particle sizes and mass flow rates for a slot size of 10 mm. Figures 10 and 11 show the effect of changing the magnitude of B on the non-dimensionalised temperature profiles obtained using the single particle model.

Figure 10 B estimation for single particle model (see online version for colours)

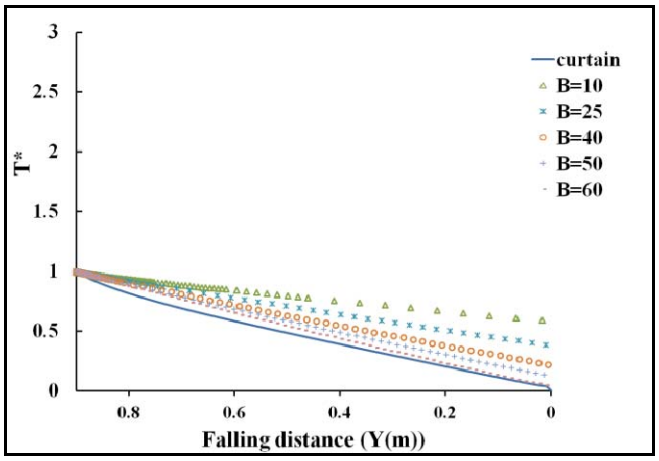

Notes: Slot opening size = 10 mm, d_s = 600 μm, m^o = 0.041 kg/s

Figure 11 B estimation for single particle model (see online version for colours)

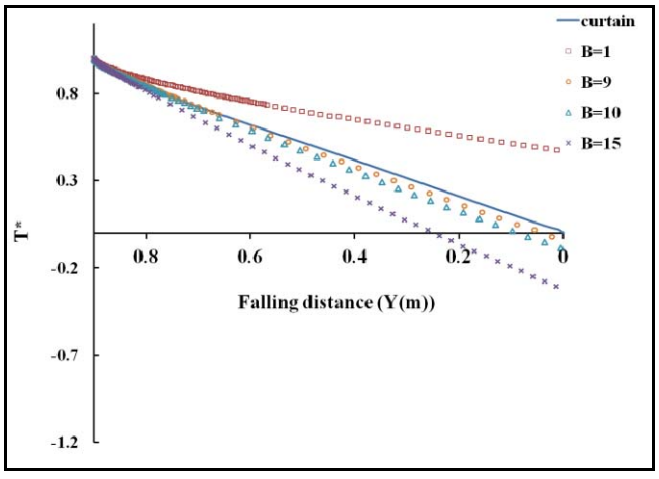

Notes: Slot opening size = 10 mm, d_s = 400 μm, m^o = 0.1 kg/s

Using the initial estimates as starting guesses, B values were optimised by adopting a MATLAB routine in which a derivative-free search procedure was employed. The objective function was defined as the sum of the absolute differences between the non-dimensionalised centreline

temperatures obtained using the ROM (single particle model) and that obtained from the CFD simulation [equation (40)].

$$\text{Objective function} = \sum \left| T^*_{CFD} - T^*_{SingleParticle} \right| \tag{40}$$

To minimise the difference between the two temperature profiles the same number of temperature data points were required at equal falling distance. There were 100 discrete CFD data points in each profile. The single particle model results were interpolated to provide the same number of data points at the required distances. Figure 12 shows the estimated values of B for best match between the ROM and the CFD profiles.

Figure 12 Parameter estimation for B values using equation (39) (see online version for colours)

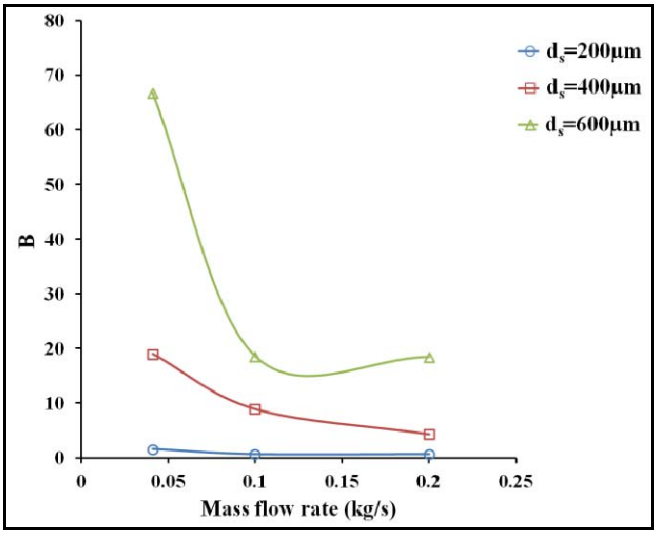

Figure 12 demonstrates that there is less change in drag coefficient of single particle at lowest particle size, as expected. As the particle size is increased the drag coefficient is increased. At low mass flow rate a higher drag coefficient is required, independent of particle size.

The CurveExpert Professional software was used to extract a correlation between mass flow rate, particle size and B [equation (41)].

$$B = \frac{-20.19 + 65.254 m^o + 90{,}175.1 d_s}{1 + 22.045 m^o - 2{,}257.49 d_s} \tag{41}$$

8 Conclusions

CFD simulations have been used to predict the heat transfer and temperature profiles within particle curtains with different mass flowrates (0.041 kg/s, 0.1 kg/s, 0.2 kg/s) discharging through different widths slots (10 mm, 60 mm, 80 mm). The CFD results have been compared to the temperature of single particle falling under equivalent conditions. It was found that the heat loss within the particle curtains is less than the equivalent single particle heat loss, as expected. As the mass flow rate of the particle curtains increases, the rate of heat loss decreases. Heat loss per unit mass decreased by a maximum of 13% by decreasing curtain width from 80 mm to 10 mm. However, CFD simulations show that there is a limit to the potential increase in heat transfer as initial curtain width increases. Analysis of variance was used to predict the most significant effects on the rate of heat loss. The three top significant variables were mass flow rate and particle size and the interaction of these variables. Temperature profiles using both CFD and single particle models were generated. CFD results were well matched with single particle at low mass flow rates and small particle sizes. Single particle model was not able to predict the behaviour of particles in curtains at larger particle sizes. A ROM correlation was developed using the single particle model as a basis. The magnitude of the drag coefficient was varied for different mass flow rates and particle sizes at slot size of 10 mm. It was observed that the magnitude of drag coefficient is higher for larger particle sizes and lower mass flow rates.

References

Afshar, S. and Sheehan, M. (2013) 'CFD and experimental study of convectional heat transfer in free falling particle curtains', Paper presented at the *11th ICNAAM*, 21–27 September, Rhodes, Greece.

Baker, C.G.J. (1992) 'Air-solids drag in cascading rotary dryers', *Drying Technol*., Vol. 10, No. 2, pp.365–393.

Britton, P.F., Sheehan, M.E. and Shneider, P.A. (2006) 'A physical description of solids transport in flighted rotary dryers', *Powder Technol*., Vol. 165, No. 3, pp.153–160.

CurveExpert Professional 2.0.0 [online] http://www.curveexpert.net/products/curveexpert-professional/.

Gidaspow, D. (1994) *Multiphase Flow and Fluidization*, Academic Press, San Diego.

Hurby, J., Steeper, R., Evans, G. and Crowe, C. (1988) 'An experimental and numerical study of flow and convective heat transfer in freely falling curtain of particles', *J. Fluid. Eng-T. ASME*, Vol. 110, No. 2, pp.172–181.

Incropera, F.P. and DeWitt, D.P. (2002) *Fundamentals of Heat and Mass Transfer*, 5th ed., John Wiley & Sons, Inc., New York.

Kim, K., Siegel, N., Kolb, G., Rangaswamy, V. and Moujaes, S.F. (2009) 'A study of solid particle flow characterization in solar particle receiver', *Sol. Energy*, Vol. 83, No. 10, pp.1784–1793.

Ogata, K., Funatsu, K. and Tomita, Y. (2001) 'Experimental investigation of a free falling powder jet and the air entrainment', *Powder Technol*., Vol. 115, No. 1, pp.90–95.

Papadikis, K., Gu, S. and Bridgwater, A.V. (2009) 'CFD modelling of the fast pyrolysis of biomass in fluidised bed reactors. Part B: heat, momentum and mass transport in bubbling fluidised beds', *Chem. Eng. Sci*., Vol. 64, No. 5, pp.1036–1045.

Pei, P., Zhang, K. and Wen, D. (2012) 'Comparative analysis of CFD models for jetting fluidized beds: the effect of inter-phase drag force', *Powder Technol*., Vol. 221, pp.114–122.

Ranz, W.E. and Marshall, W.R. (1952) 'Friction and transfer coefficients for single particles and packed beds', *Chem. Eng. Prog*., Vol. 48, No. 3, pp.247–253.

Schiller, L. and Naumann, A. (1933) 'Über die grundlegenden Berechnun gen bei der Schwekraftaubereitung', *Z. Ver. Dtsch. Ing.*, Vol. 77, pp.318–320.

Thanh, T.B., Will Cox, K. and Ghattas, O. (2008) 'Parametric reduced-order models for probabilistic analysis of unsteady aerodynamic applications', *AIAA J.*, Vol. 46, No. 10, pp.2520–2529.

Wardjiman, C. and Rhodes, M. (2009) 'Heat transfer in a particle curtain falling through a horizontally-flowing gas stream', *Powder Technol.*, Vol. 191, No. 3, pp.247–253.

Wardjiman, C., Lee, A., Sheehan, M. and Rhodes, M. (2008) 'Behaviour of a curtain of particles falling through a horizontally-flowing gas stream', *Powder Technol.*, Vol. 188, No. 2, pp.110–118.

Wardjiman, C., Lee, A., Sheehan, M. and Rhodes, M. (2009) 'Shape of a particle curtain falling in stagnant air', *Powder Technol.*, Vol. 192, No. 3, pp.384–388.

Wen, C.Y. and Yu, Y.H. (1966) 'Mechanics of fluidization', *Chem. Eng. Prog. Symp. Sries*, Vol. 62, No. 2, pp.100–111.

Zhang, K., Zhang, J. and Zhang, B. (2004) 'CFD simulation of jet behaviour and voidage profile in a gas-solid fluidized bed', *Int. J. Energy Res.*, Vol. 28, No. 12, pp.1065–1074.

Nomenclature

A	Area (m^2)
C_D	Drag coefficient (-)
C_p	Specific heat capacity ($J.kg^{-1}.K^{-1}$)
d	Diameter (m)
e_s	Restitution coefficient of particles (-)
F_D	Drag force (N)
F_G	Gravity force (N)
g	Acceleration due to gravity, 9.81 ($m.s^{-2}$)
g_0	Radial distribution function (-)
$G_{kb,g}$	Turbulent production due to buoyant forces ($kg.m^{-1}.s^{-3}$)
$G_{k,g}$	Turbulent production due to viscous and buoyant forces ($kg.m^{-1}.s^{-3}$)
h	Convective heat transfer coefficient ($W.m^{-2}.K^{-1}$)
$\bar{\bar{I}}$	Unit stress tensor (-)
k	Thermal conductivity ($W.m^{-1}.K^{-1}$)
k	Turbulence kinematic energy per unit mass ($m^2.s^{-2}$)
m	Mass (kg)
m^o	Mass flow rate ($kg.s^{-1}$)
P	Pressure (pa)
Pr	Prandtl number (-)
Re	Reymolds number (-)
T	Transpose (-)
T	Temperature (K)
T^*	Non-dimensionalised temperature (-)
t	Time (s)
v	Velocity ($m.s^{-1}$)
v'	Fluctuating velocity ($m.s^{-1}$)
Greek letters	
α	Volume fraction (-)
β	Interphase drag coefficient ($kg.m^{-3}.s^{-1}$)
ε	Turbulence dissipation rate ($m.s^{-3}$)
Θ_s	Granular temperature ($m^2.s^{-2}$)
λ	Bulk viscosity (pa.s)
μ	Dynamic viscosity ($kg.m^{-1}.s^{-1}$)
ρ	Density ($kg.m^{-3}$)
$\bar{\bar{\tau}}$	Stress tensor (pa)
Subscripts	
f	Final
g	Gas phase
p	Phase type (solid or gas)
q	Phase type (solid or gas)
s	Particle phase
tr	Turbulent
xs	Cross-sectional-/projected